ACS OMEGA

http://pubs.acs.org/journal/acsodf

Article

UiO66-Derived Catalyst for Low Temperature Catalytic Reduction of NO with NH_3

Ka-Ming Leung, Chi-Kin J. Tsui, Ching-Kit Ho, Chang-Zhong Liao, Hei-Tung Yau, Kwong-Yu Chan,* and Chi-Ying V. Li*

Cite This: *ACS Omega* 2023, 8, 12362−12371

Read Online

ACCESS | Metrics & More | Article Recommendations | Supporting Information

ABSTRACT: Diesel exhaust emissions are major outdoor air pollutants. Reducing the emission of NOx by diesel commercial vehicles and related machineries is at present a great challenge. In this study, we synthesize a catalyst for low-temperature catalytic reduction of NO using calcinated UiO-66(Zr) as a host for the doping of cerium, manganese, and titanium by the incipient wetness impregnation, followed by the dispersion of 1.0 wt % platinum. A solid solution of $Ce_{0.15}Zr_{0.54}Mn_{0.11}Ti_{0.20}O_2$/1.0Pt (CZMTO/Pt) is synthesized as evident by the structural characterizations. The catalyst demonstrates significant NO reduction in the laboratory due to the synergistic effect of various elements, with NO conversion above 80% at 160 °C.

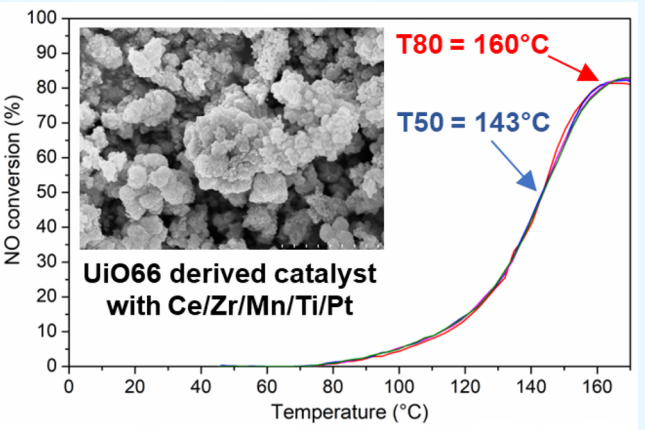

INTRODUCTION

The emission of nitrogen oxides (NOx) from power plants and automobiles is one of the major causes leading to various environmental issues such as chemical smog, acid rain, and the greenhouse effect. Selective catalytic reduction (SCR) of NOx using ammonia or urea is still the most effective technology to remove NOx and has been widely adapted by industries for many decades.[1] Among all types of catalysts being developed, conversational vanadium-based catalyst (V_2O_5) has been commercialized and widely used in NH_3-SCR of NOx due to its SO_2 and H_2O resistance.[2,3] However, vanadium is highly toxic in its inorganic form and is harmful to the environment.[4] Other drawbacks of vanadium-based catalysts (i.e., V_2O_5−WO_3/TiO_2) include a relatively narrow optimal SCR temperature range (300−400 °C) and they are readily poisoned by alkali salt from the exhaust gases.[5,6] Therefore, tremendous efforts have been made to either reduce the vanadium content of SCR catalyst or search for alternatives to replace vanadium, as well as to improve SCR performance at low temperature.

Various metal oxides have been proposed as SCR catalysts.[7,8] Among these catalysts, cerium-containing oxides have been extensively studied due to their relatively low cost and environmental friendliness.[9] Moreover, cerium-based catalysts show excellent oxygen storage capacity due to the presence of oxygen vacancies arising from the redox couple between Ce(III) and Ce(IV) under both oxidizing and reducing conditions.[10,11] The adsorption of NO/NH_3 species on the catalytic surface can therefore be enhanced due to the increases in surface acidity. However, the catalytic activity of CeO_2 alone, without doping of other transition metals, shows unsatisfactory NO conversion.[12] Even with the doping of transition metals, the typical NOx conversion temperatures (above 80%) for these cerium-based metal oxides are above 200 °C.[13] It is evident that introducing manganese as a dopant can further ameliorate the NH_3-SCR performance at low temperature due to the synergistic effects between cerium and manganese.[14]

Zirconium (Zr) and titanium (Ti) are two other common transition metals present in multimetal NH_3-SCR catalyst, either as active components or active support materials.[15] Zirconium is known to improve the thermal stability of cerium-based catalyst by maintaining porosity and minimizing particle sintering at high temperature.[16−18] Meanwhile, titanium in the form of TiO_2-anatase has excellent SO_2 tolerance by inhibiting the formation of sulfate salt on the catalytic surface.[19,20] Trace of noble metals (less than 1.0 wt %) such as platinum can also be added to the multimetal catalysts to further lower the NH_3-SCR temperature.[21,22] In general, the distinct role of the

Received: January 9, 2023
Accepted: January 30, 2023
Published: March 24, 2023

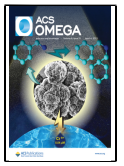

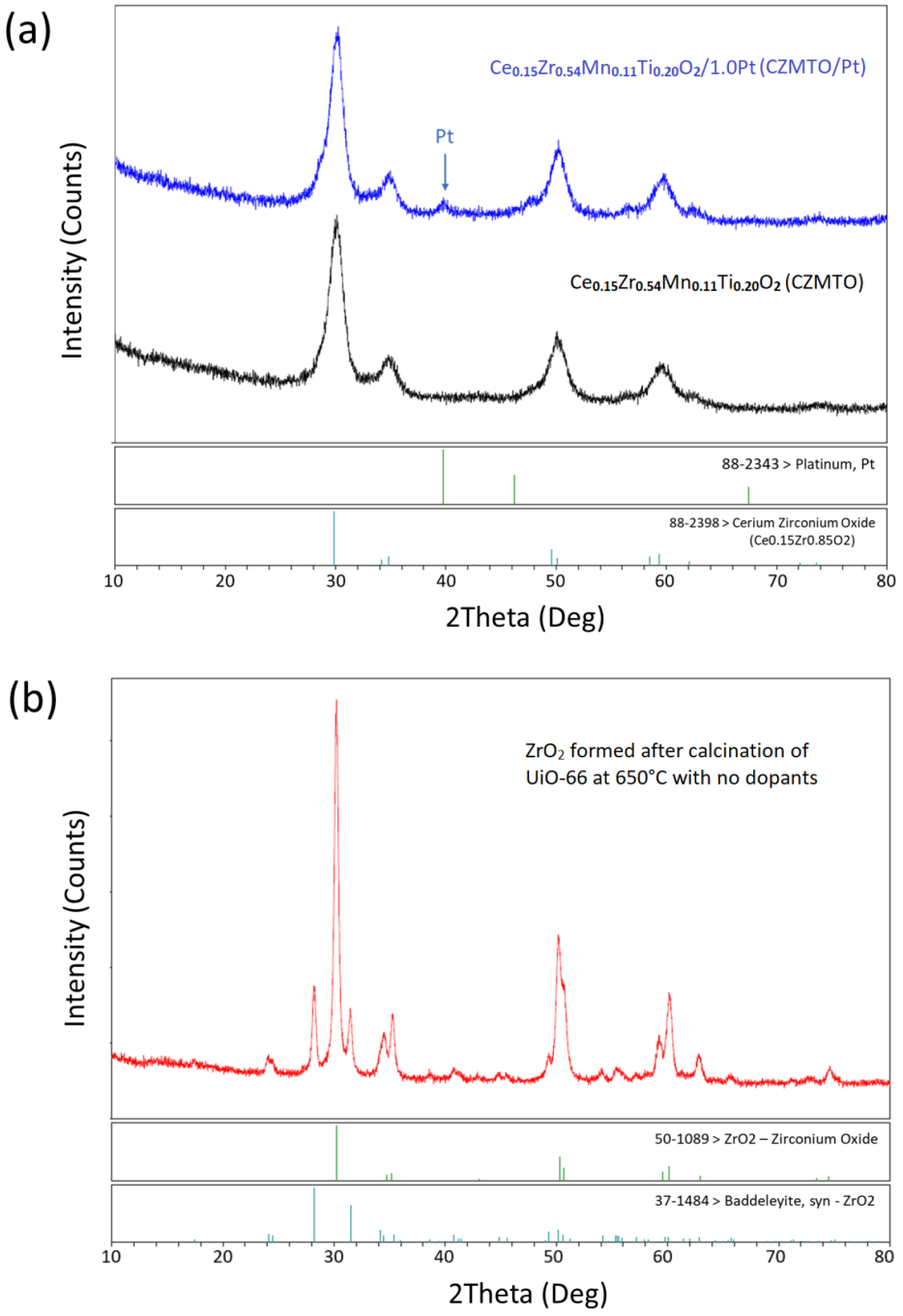

Figure 1. (a) XRD patterns of CZMTO/Pt (blue) and CZMTO (black). Standard XRD patterns of $Ce_{0.15}Zr_{0.85}O_2$ (PDF 88-2398) and platinum (PDF 88-2343) are also included for reference. (b) XRD pattern of UiO-66 without addition of dopant precursors after heat treatment in air at 650 °C for 180 min.

individual metal component of a multimetal catalyst cannot be clearly defined, but rather the synergistic effects of all these elements create a colossal of oxygen vacancies, redox properties, and active site acidities, leading to the superior low temperature NO reduction performance of these multimetal catalysts.

Apart from varying the transition metal composition of NH_3−SCR catalysts, different preparation methods are also known to improve NOx reduction efficiency. Depending on the methods of catalyst synthesis (i.e., coprecipitation, templating, impregnation, etc.), the specific surface area, porosity, and morphology (crystallinity and particle size uniformity) can be controlled, which can facilitate NH_3-SCR at low temperature.[23] Several challenges still exist when preparing these multimetal catalysts. The formation of an inhomogeneous composite with the presence of segregated metal oxide phase could eventually lead to poor NOx reduction performance. In addition, a significant decrease in specific surface area after calcination at high temperature is not uncommon during catalyst preparation, as a result of particle sintering.[24] Since the specific surface area corresponds to the number of active sites exposed on the surface of the catalyst, it

https://doi.org/10.1021/acsomega.2c07110
ACS Omega 2023, 8, 12362−12371

is important to improve thermal resistance to avoid catalyst degradation and loss of surface area under high temperature calcination conditions during sample preparation.

Herein, we report the first zirconium-based catalyst utilised a UiO-66 metal organic framework derived host for NO reduction. UiO-66 MOF is also acting as a source of zirconium for the catalyst. Cerium, manganese, and titanium are doped to UiO-66 via an incipient wetness impregnation method. The as-synthesized catalyst is thermally stable and retains a comparable BET surface area after calcination at 650 °C, forming a solid solution with no phase segregation, and resembles the morphology of UiO-66. Catalyst with 1.0 wt % Pt dispersion achieves T_{50} below 150 °C and T_{80} at around 160 °C for NO reduction in presence of NH_3.

RESULTS AND DISCUSSION

Characterization of UiO-66. UiO-66 is successfully synthesized using a hydrothermal method as evident from the XRD, SEM, and BET analysis. In this study, two types of Zr precursors ($ZrCl_4$ and $ZrO(NO_3)_2$) are used for the UiO-66 synthesis (details can be found in the Experimental Section) and the corresponding XRD patterns shown in Figure S1. The XRD powder pattern of all as-synthesized UiO-66 matches well with the commercially available sample. However, a broad peak with low intensity centered at 21° 2θ is observed for the commercial sample, which indicates the presence of amorphous material or impurities. The intensity of such a broad peak reduces dramatically for the samples synthesized on a laboratory scale, using either $ZrCl_4$ or $ZrO(NO_3)_2$ as precursors. Under identical synthesis conditions, UiO-66 synthesized using $ZrCl_4$ has diffraction peaks with stronger intensities, which indicates a better crystallinity compared to the sample synthesized using $ZrO(NO_3)_2$. The better crystallinity could be attributed to the solubility of the Zr precursors as observed during the synthesis; a clear solution is formed using $ZrCl_4$, while the solution using $ZrO(NO_3)_2$ remains opaque after prolong stirring (i.e., 24 h). Several diffraction peaks with stronger intensities at 7.3, 8.5, 12.0, 17.0, 20.9, 22.3, 25.7, 30.8, and 20.9° 2θ can be assigned to the (111), (002), (022), (004), (115), (044), (006), and (117) lattice planes of UiO-66, respectively. It can be concluded from the XRD data that UiO-66 synthesized using $ZrCl_4$ (hereafter represent all UiO-66 being mentioned) would give better crystallinity with a minimum amount of impurities and thus is chosen as the host for the UiO-66-derived catalyst.

The morphology and porosimetry of the as-synthesized UiO-66 is presented in Figure S2. Aggregation of particles less than 0.1 μm in spherical shape are observed in the SEM image (Figure S2a). UiO-66 exhibits a reversible Type 1(b) isotherm with a small H1 hysteresis loop closed to ambient pressure (Figure S2b). Such an isotherm is typical for solids that contain both wider micropores and narrow mesopores (≤2.5 nm).[25,26] The measured Brunauer–Emmett–Teller (BET) surface area and pore volume are 1302 $m^2\ g^{-1}$ and 0.77 $cm^3\ g^{-1}$ respectively. Such high surface area and pore volume might attribute to the linker defect induced by the amount of conc. HCl used as the modulator and is beneficial for the impregnation of various metal precursors for the catalyst synthesis.[27]

Characterization of Catalyst (CZMTO/Pt). UiO-66 is used as a host for the synthesis of CZMTO/Pt by an incipient wetness impregnation method due to the presence of zirconium in UiO-66 with the addition of Ce, Mn, and Ti precursors in relative ratios. The UiO-66 framework is decomposed during calcination at 650 °C (details of the synthesis can be found in the Experimental Section). In theory, any MOFs with the desired metal ions, i.e., Ce/Ti/Mn/Zr-containing MOFs, can be applied as the host for the synthesis.

Structure, Composition, and Morphology. The structure of as-synthesized CZMTO/Pt catalyst is analyzed by XRD (Figure 1a). The powder pattern of pristine $Ce_{0.15}Zr_{0.54}Mn_{0.11}Ti_{0.20}O_2$ (CZMTO) before Pt impregnation is also included for comparison. All patterns match the cubic phase of ZrO_2 with unit cell parameter a = 5.128 Å (PDF 49-1642). Due to the doping of a small amount of Ce, Mn, and Ti and the slightly broadened nature of the diffraction peaks, the powder patterns could also fit several tetragonal $Ce_{1-x}Zr_xO_2$ solid solutions with compositions, for example, $Ce_{0.15}Zr_{0.85}O_2$ (PDF 88-2398), $Ce_{0.14}Zr_{0.86}O_2$ (PDF 38-1437), and $Ce_{0.12}Zr_{0.88}O_2$ (PDF 82-1398).

However, from the EDX analysis (data present in a later section), the Ce/Zr/Mn/Ti ratio of the catalyst together with the XRD pattern are very close to the tetragonal phase of $Ce_{0.15}Zr_{0.85}O_2$ (PDF 88-2398) (Figure 1a). Therefore, a solid solution is being synthesized. The Ti and Mn are incorporated into the structure and replace some Zr sites within the lattice since neither segregated anatase/rutile nor manganese oxide peaks are observed from all powder patterns. Moreover, no CeO_2 and Ce_2O_3 phases are being detected. There is also no structural change after impregnation with 1.0 wt % Pt black, but a small platinum (111) peak located at 40° 2θ indicates the presence of platinum (PDF 88-2343).

When as-synthesized UiO-66 is calcined at 650 °C for 180 min with no addition of dopant precursors, two phases of ZrO_2 are formed (Figure 1b) — tetragonal zirconium oxide (PDF 50-1089) and monoclinic baddeleyite (PDF 37-1484). Therefore, the doping of Ce/Mn/Ti into UiO-66 provides not only the synergistic effect for the NO reduction but also promotes a homogeneous, single-phase structure for the catalyst being synthesized.

The morphology of CZMTO/Pt is analyzed using SEM (Figure 2a). The SEM image of CZMTO is also included for comparison (Figure 2b). There are no significant changes in morphology before and after Pt impregnation. Aggregation of nanosized particles which resemble the morphology of UiO-66 host (Figure S2a) is observed. This implies that the morphology of the catalyst can be designed by using a host with the desired morphology.[28] The EDX data of CZMTO/Pt and CZMTO are summarized in Table 1. There is no significant difference in the average atomic % of the components before and after Pt impregnation. Unfortunately, Pt cannot be detected/quantified by EDX mapping with the presence of Zr, as the EDX signals of Zr and Pt overlap with each other. Such Pt/Zr overlap can also explain the slightly

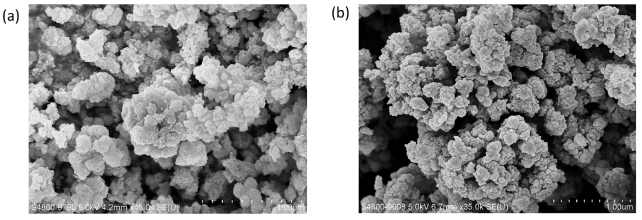

Figure 2. SEM Images of (a) CZMTO/Pt (b) CZMTO.

https://doi.org/10.1021/acsomega.2c07110
ACS Omega 2023, 8, 12362−12371

Table 1. SEM-EDX Analysis of CZMTO Catalyst before and after Pt Impregnation

	Average atomic % (at. %)			
Catalyst	Ce	Zr	Mn	Ti
CZMTO/Pt	14.5	54.4	10.7	20.4
CZMTO	15.3	51.9	10.9	21.9

increase in Zr content (decrease in Ce/Mn/Ti) after Pt impregnation as the Zr atomic % is the sum of Zr and Pt.

The HR-TEM image of CZMTO/Pt is shown in Figure 3a. The selected area electron diffraction (SAED) (Figure 3b, inset) shows a concentric circular pattern suggesting that the catalyst is polycrystalline. The calculated *d*-spacings from the SAED pattern match the tetragonal $Ce_{1-x}Zr_xO_2$ solid solution ($x \geq 0.8$) (Table 2). However, the measured *d*-spacing from the HR-TEM image shows a rather wide range (average of 0.320 nm) compared to those calculated from SAED (0.296 nm for *hkl* [101]). Such a difference in *d*-spacing might due to the random substitution of Ce/Ti/Mn to the ZrO_2 lattice, since the ionic radii of Ce/Ti/Mn are different from that of Zr, i.e., 101 pm for Ce^{4+} versus 86 pm for Zr^{4+}, which might cause some expansion to the lattice planes. No Pt particles are observed by HR-TEM because of the low Pt content. Pt might also be dispersed on an atomic scale which is too small for TEM characterization. The presence of Pt, however, is evident by the X-ray photoelectron spectroscopy (XPS) characterization in a later section. CZMTO/Pt shows a uniform particle size distribution with an average particle size of 16.1 nm (Figure 3c) and is present as agglomerates.

Table 2. Calculated d-Spacings from SAED of CZMTO/Pt (Figure 3b, Inset) Assigned to the Corresponding $Ce_{0.15}Zr_{0.85}O_2$ Lattice Planes (PDF 88-2398)

Concentric ring no. from SAED	Calculated *d*-spacing (nm)	Corresponding Miller index (hkl) $Ce_{0.15}Zr_{0.85}O_2$
1	0.296	101
2	0.263	110
3	0.181	200
4	0.154	211
5	0.128	220

Specific Surface Area and Pore Structure. The nitrogen sorption isotherms of CZMTO/Pt (Figure 4) are significantly different compared to as-synthesized UiO-66 (Figure S2b). The catalyst has a reversible type 2 isotherm which is typical for macroporous adsorbent, and the H3 hysteresis loop indicates the catalyst has aggregates of platelike particles forming slitlike pores.[25,26] The BET surface area is measured to be 42.7 $m^2\ g^{-1}$ with a pore volume of 0.14 $cm^3\ g^{-1}$. The significant drop in BET surface area (97%) and pore volume (82%) of the catalyst compared to UiO-66 is in agreement with the isotherm, showing a collapse of the framework to form the solid solution and a loss of microporosity.

Surface Chemical State. The surface oxidation states and elemental concentration of CZMTO/Pt is characterized by XPS. Table S1 summarizes the data collected from XPS after background removal, including the binding energy, full width at half-maximum (fwhm), chemical states, and relative atomic % of the composed elements, with the corresponding high-resolution core level spectra presented in Figure 5.

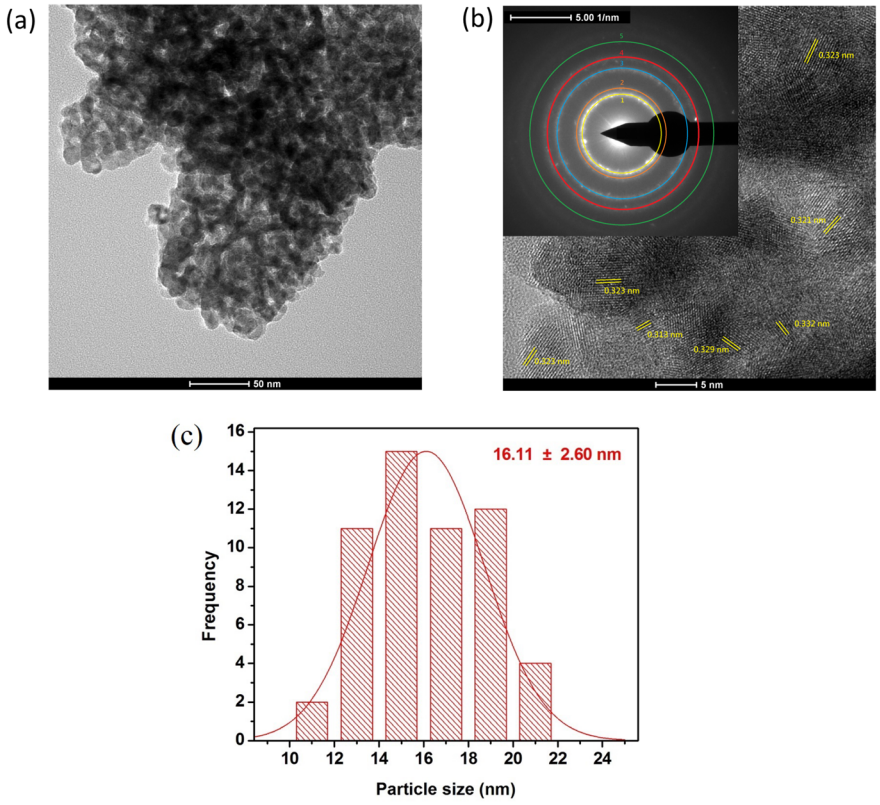

Figure 3. HR-TEM image of (a) CZMTO/Pt and (b) with measured *d*-spacings and the corresponding SAED shown as an inset. (c) Particle size distribution of CZMTO/Pt calculated using the HR-TEM image (a).

https://doi.org/10.1021/acsomega.2c07110
ACS Omega 2023, 8, 12362−12371

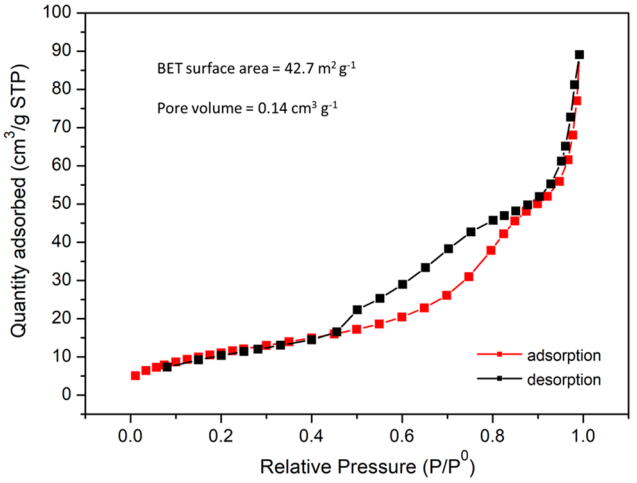

Figure 4. N_2 sorption isotherms of CZMTO/Pt.

The Ce 3d core level spectrum (Figure 5a) shows four pairs of doublets, with peaks u3, u2, u1, u and v3, v2, v1, v assigned to the Ce 3d3/2 and Ce 3d5/2 chemical states, respectively.[29,30] The doublet pairs of (u3/v3), (u2/v2), and (u/v) can be ascribed to the diversified Ce^{4+} species, while the (u1/v1) doublet can be ascribed to Ce^{3+}. The amount of Ce^{3+} (u1 + v1) is approximately 25% of all the Ce present on the surface of the catalyst, with a Ce^{3+} to Ce^{4+} ratio of 0.33.

The O 1s core level spectrum (Figure 5b) shows two oxygen chemical states on the surface of the catalyst. The peaks at 531.57 and 529.75 eV correspond to the surface-adsorbed oxygen species (Oα) and the surface lattice oxygen species (Oβ), respectively.[31] No bulk lattice oxygen is detected. The relative concentration of Oα is 19.6%, with a Oα/Oβ ratio of 0.25. Surface-adsorbed oxygen, Oα, is related to the oxygen vacancy created by the presence of Ce^{3+} and involved in the redox cycle of Ce^{4+}/Ce^{3+} of NO reduction.

From the Zr 3d core level spectrum (Figure 5c), the doublet pair at 184.47 and 182.09 eV can be assigned to Zr 3d3/2 and Zr 3d5/2, respectively.[32,33] The doublet corresponds to the Zr(IV) oxide phase, and no metallic Zr(0) (178.9 eV for Zr 3d5/2) is detected. The same pattern is also observed for the Ti 2p (Figure 5d) and Mn 2p spectra (Figure 5e). The doublet pair at 653.35 and 641.52 eV of the Mn 2p spectrum can be ascribed to Mn 2p1/2 and Mn 2p3/2, respectively, while the doublet pair of the Ti 2p spectrum at 464.03 and 458.33 eV can be ascribed to the Ti 2p1/2 and Ti 2p3/2, respectively.[32,33] Although Ti is presented as Ti(IV) oxide, it is not in segregated in rutile or anatase form, since no such phases are observed in the XRD pattern. The same also applies to Mn which presents as either Mn(III) or Mn(IV); no segregated Mn_2O_3 and MnO_2 phases are observed in the powder pattern. Moreover, in both cases, no XPS state related to the metallic Ti(0) and Mn(0) is detected, and thus Ti and Mn are incorporated into the ZrO_2 lattice.

Due to the very low concentration of Pt present in the catalyst, the peaks in the Pt 4f spectrum are difficult to resolve. However, the XPS survey spectrum indicated that the relative atomic % of Pt calculated from the Pt 4f scan is 0.12. Moreover, Pt should be presented in metallic form, since a Pt (111) peak is observed in the XRD (Figure 1a), and no oxide form is detected.

The surface dopant composition (Ce, Ti, Mn) of CZMTO/Pt obtained from XPS analysis (Table S1) is also compared to its bulk derived from SEM-EDX (Table 1), as shown in Table 3. Pt is not included since metallic Pt (Pt black) is added, which should not incorporate into the ZrO_2 lattice. In general, the surface of the catalyst has a higher concentration of Ce, Mn, and Ti as dopants; Ce on the surface is nearly doubled compared to the bulk, while Mn and Ti on the surface are about 3 times compared to the bulk. The higher dopant concentration on the surface is likely due to the uneven absorption of dopant solution by UiO-66 via capillary action during sample preparation. However, such a relatively high dopant concentration on the surface of the catalyst would promote the interaction between NO/NH_3 and the synergistic effect of the doping ions, thus improving the NO reduction ability of the catalyst.

Catalytic Performance of CZMTO/Pt in NO Reduction. The NO reduction performance of CZMTO/Pt is analyzed using online mass spectroscopy for potential application in automobile catalytic converters. The setup, testing conditions, as well as the NO conversion derived from the mass spectrometry signal are outlined in the Experimental Section. The NO reduction performance of the catalyst before and after Pt impregnation are compared using the 50% (T_{50}) and 80% (T_{80}) conversion temperature, where T_{50}/T_{80} is the temperature at which NO conversion can reach 50%/80%. Table 4 summarizes the T_{50}, T_{80}, T_{max}, and the maximum percentage NO conversion of the catalyst. Five cycles and two cycles were tested for CZMTO/Pt and CZMTO respectively, and the results are shown in Figure 6.

CZMTO/Pt (Figure 6a) shows consistent NO conversion temperature from second to fifth cycles with T_{50} at 143 °C and T_{80} at 160 °C. There are small improvements on the maximum % NO conversion (approximately 1.5%) comparing the fifth cycle to the second cycle. The deviation of the first cycle is due to the activation of the catalyst; for example, the chemical state of different dopants on the surface will need to be established before a stable performance can be maintained. On the other hand, CZMTO shows an increase in T_{50} for both cycles (Table 4). The NO reduction is believed to be ongoing, since no plateauing in performance before/at 220 °C is observed. From the NO reduction results, it is evident that Pt plays a role in reducing the NO conversion temperature.

The low-temperature NO reduction facilitated by the catalyst CZMTO/Pt can also be attributed to the doping of cerium. The presence of Ce^{3+} (as evident from the XPS analysis) is related to the formation of oxygen vacancies on the surface of the catalyst. The oxygen vacancies created by the Ce^{3+} promote adsorption of oxygen and, through electron transfer between Ce and O species, further enhance the reversible redox couple between Ce^{3+} and Ce^{4+}. Ce^{3+} can also act as a Lewis acid site for the adsorption of ammonia. Some mechanisms suggested that during the NO reduction cycle NO is not adsorbed directly on the surface of the catalyst, but instead, on the ammonia species adsorbed on the surface of the catalyst (i.e., NO-NH_2-CeOH).[31] The presence of Ce^{3+} on the surface enhanced both the acidic and redox property of the catalyst and, thus, the NO reduction performance.

CONCLUSION

The catalyst with composition $Ce_{0.15}Zr_{0.54}Mn_{0.11}Ti_{0.20}O_2$/1.0Pt (CZMTO/Pt) is successfully synthesized via an incipient wetness impregnation method using a UiO-66-derived host

https://doi.org/10.1021/acsomega.2c07110
ACS Omega 2023, 8, 12362−12371

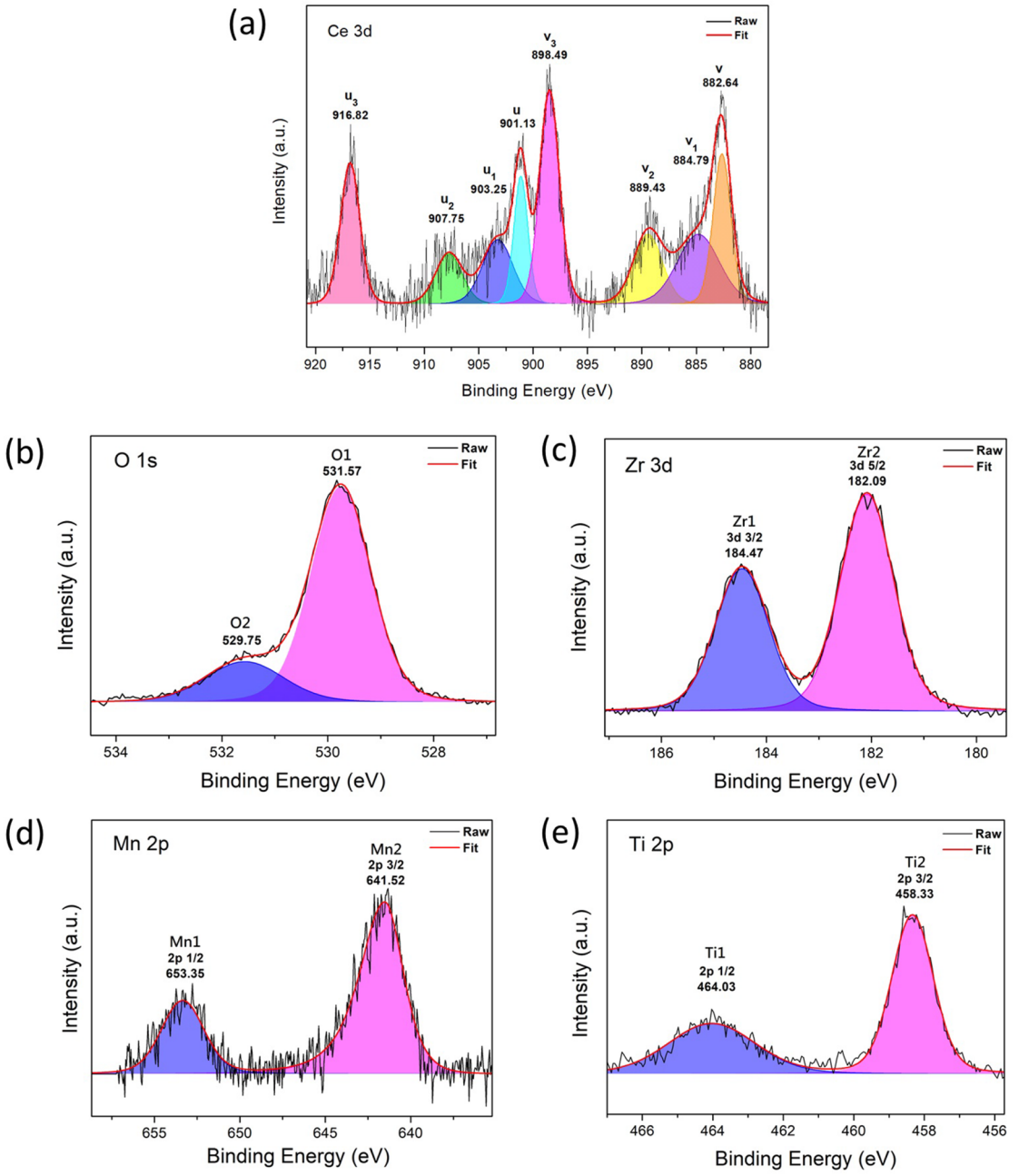

Figure 5. XPS core level scans of (a) Ce 3d, (b) O 1s, (c) Zr 3d, (d) Mn 2p, and (e) Ti 2p of CZMTO/Pt.

Table 3. Surface versus Bulk Dopant Composition of CZMTO/Pt

Dopant (Corresponding to Zr)	Dopant ratio	
	Surface (from XPS)	Bulk (from SEM-EDX)
Ce/Zr	0.51	0.27
Mn/Zr	0.59	0.20
Ti/Zr	1.28	0.37

and is proved to be effective for low-temperature NO reduction with NH_3. Structural characterization shows that the catalyst is a solid solution with no phase segregation, and cerium, titanium, and manganese are successfully doped into the structure. The catalyst is also thermally stable after calcination at 650 °C, resembling the morphology of UiO-66. With the addition of 1.0 wt % Pt, the catalyst manifests significant NO conversion ability achieving T_{50} and T_{80} at 140 and 160 °C, respectively. To the best of our knowledge, this is the first catalyst being synthesized using a metal organic framework which also shows outstanding NO reduction with NH_3 at low temperature.

EXPERIMENTAL SECTION

Synthesis of Zirconium 1,4-Dicarboxybenzene Metal Organic Framework (UiO-66). UiO-66 was synthesized hydrothermally using two different zirconium precursors. The following chemicals and reagents were used as purchased without further purification. Sublimed grade zirconium(IV) chloride ($ZrCl_4$; 99.95+% - Zr) was purchased from Strem

https://doi.org/10.1021/acsomega.2c07110
ACS Omega 2023, 8, 12362−12371

Table 4. Summary of 50% (T_{50}), 80% (T_{80}), Maximum (T_{max}) NO Conversion Temperature, And the Corresponding Maximum Percentage NO Conversion of CZMTO/Pt[a]

Catalyst	Cycle	T_{50} (°C)	T_{80} (°C)	T_{max} (°C)	Max NO conversion (%)
CZMTO/Pt	1	151.3	N/A	165.9	79.8
	2	143.6	159.8	166.3	81.4
	3	143.6	159.9	168.9	82.3
	4	143.7	160.8	168.8	82.5
	5	143.6	161.7	168.9	83.0
CZMTO	1	156.4	N/A	220	75.5
	2	164.8	N/A	220	74.4

[a]Pristine CZMTO with no Pt impregnation is also included for comparison.

Chemicals; zirconium(IV) oxynitrate hydrate ($ZrO(NO_3)_2 \cdot xH_2O$; 99%) and terephthalic acid (BDC; 98%) were purchased from Sigma-Aldrich. AR grade hydrochloric acid (37%) was purchased from RCl Labscan; ACS, HPLC, dehydrous grade *N*,*N*-dimethylformamide (DMF) was purchased from Anaqua. Commercially available UiO-66 was purchased from Strem Chemicals to compare with the as-synthesized UiO-66 samples.

The protocol of UiO-66 synthesis is outlined as follows. In a 500 mL Duran glass bottle, 5.94 mmol of zirconium source, either $ZrO(NO_3)_2 \cdot xH_2O$ or $ZrCl_4$, was added to a DMF/HCl solution prepared by adding 11 mL of conc. HCl to 55 mL of DMF and stirred on a hot plate plate. In a 250 mL glass beaker, 8.25 mmol of BDC was added to 110 mL of DMF and sonicated in a water bath at room temperature for 20 min to form a clear solution. The BDC solution was then slowly added to the Duran glass bottle, sealed, and stirred for 1 h at

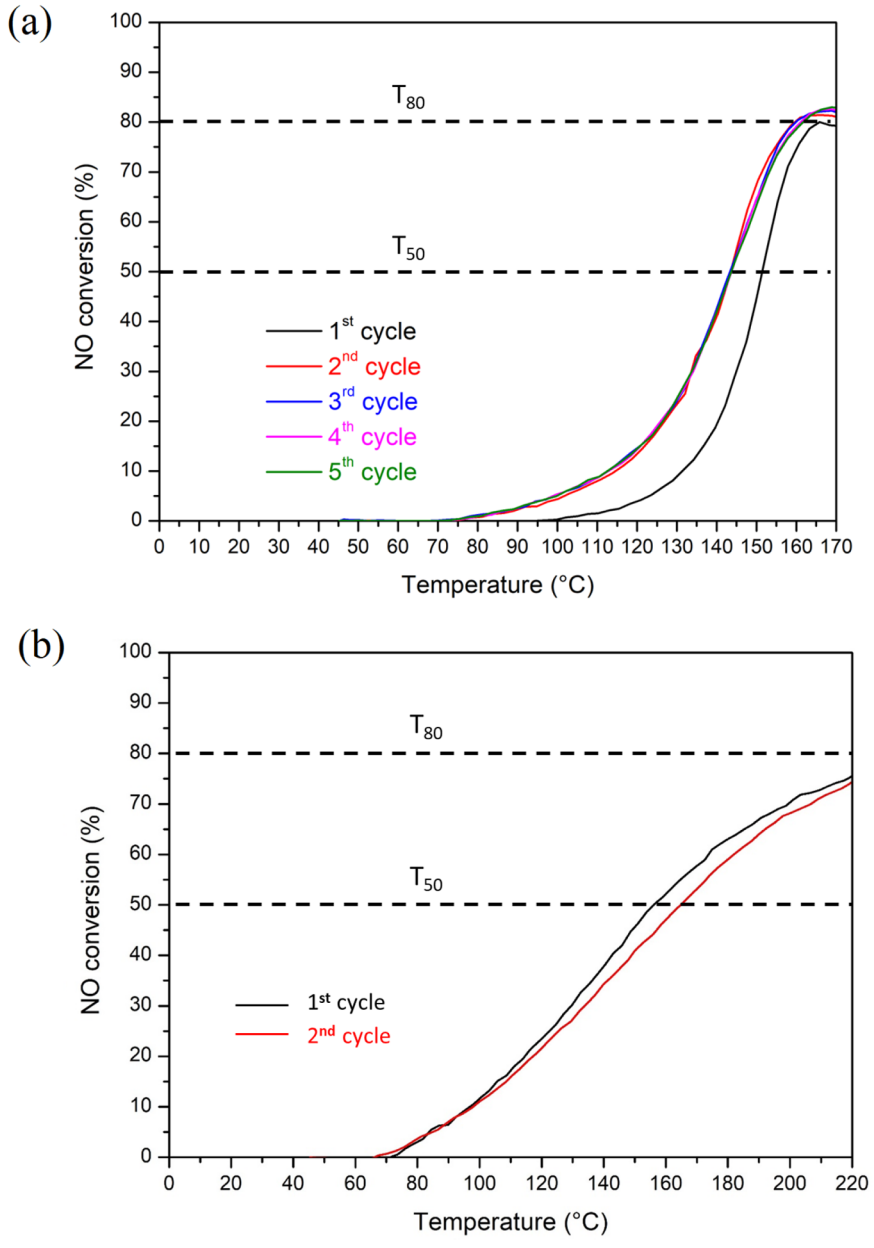

Figure 6. Percentage NO conversion plots of (a) CZMTO/Pt and (b) CZMTO.

https://doi.org/10.1021/acsomega.2c07110
ACS Omega 2023, 8, 12362−12371

85 °C on a hot plate. Thereafter, the bottle was put into a conventional oven at 85 °C for a minimum of 15 h with no stirring. The resulting mixture was centrifuged to separate the white solid, washed three times with DMF, and soaked in 300 mL of methanol for 48 h to exchange the entrapped DMF molecules within the UiO-66 framework. Finally, the white powder was separated using centrifugation (1200 rpm, 10 min) and dried in a vacuum oven at 90 °C for 24 h. A reliable yield of 1.50 g could be achieved with each synthesis.

Synthesis of Catalyst CZMTO/Pt. CZMTO/Pt was synthesized using an incipient wetness impregnation approach. The following chemicals and reagents were used as purchased without further purification. Manganese(II) nitrate hydrate ($Mn(NO_3)_2{\cdot}4H_2O$; 98%), cerium(III) nitrate hexahydrate ($Ce(NO_3)_3{\cdot}6H_2O$; 99% trace metals basis), and titanium(IV) butoxide (reagent grade, 97%) were purchased from Sigma-Aldrich.

The protocol of CZMTO/Pt synthesis is outlined as follows. 2.559 g of $Ce(NO_3)_3{\cdot}6H_2O$ and 1.125 g of $Mn(NO_3)_2{\cdot}4H_2O$ were dissolved in 26.5 mL of deionized water. The Ce/Mn solution was then added dropwise to 5.5 g of UiO-66 in a 10 cm × 10 cm × 5 cm (L*W*H) glass container. The glass container was covered with parafilm to avoid spilling, and the slurry was stirred on a hot plate at room temperature for a minimum of 60 min. The container was then placed in a conventional oven at 80 °C for 90 min to evaporate water before being placed in a vacuum oven at 40 °C overnight to form a pale brown powder. The resulting pale brown powder was ground using a mortar and pestle, and the aforementioned procedure was repeated by adding a solution prepared using 2.474 g of titanium(IV) butoxide mixed with 20 mL of ethanol. The Ce/Mn/Ti-impregnated UiO-66 powder was then sintered using a conventional oven at 650 °C for 180 min with a ramp rate of 10 °C per minute from 25 to 650 °C. A reliable yield of approximately 4.0 g of catalyst can be achieved per synthesis.

The addition of platinum (Pt) was achieved by mixing the desired amount of the as-synthesized catalyst with Pt black (1.0 wt %) and ethanol to form a slurry and thereafter sonicated in a water bath for a minimum of 60 min. The slurry was then dried in a conventional oven at 80 °C for 90 min to evaporate excess ethanol before being placed in a vacuum oven at 40 °C overnight.

Materials Characterization. The structure and composition of the as-synthesized samples are characterized using various techniques. High-resolution X-ray diffraction (HR-XRD) is performed using a Bruker D8 Advance X-ray powder diffractometer equipped with Cu Kα radiation (λ = 1.5418 Å) at 40 kV and 40 mA and a LynxEye detector. The morphologies are analyzed by scanning electron microscopy (SEM) (Hitachi S-4800 with an accelerating voltage of 7 kV coupled with an energy-dispersive X-ray spectroscopy system) and transmission electron microscopy (TEM) (FEI TECNAI G2 f20 S-twin with an accelerating voltage of 200 kV). The porosimetry is determined using a Micromeritics ASAP 2020 instrument. The sample is degassed at 200 °C and 10^{-6} Torr vacuum to remove adsorbed impurities and loaded into the analyzer to obtain the Brunauer−Emmett−Teller (BET) surface area and pore volume. The analysis is carried out at 77 K with liquid nitrogen as the adsorbent gas. X-ray photoelectron spectroscopy (XPS) is carried out to analyze the surface state of the catalyst using a Thermo Fisher Scientific Kα X-ray photoelectron spectrometer system with a monochromated Al Kα X-ray source (1.487 keV) at a base pressure of 210^{-9} mbar. The survey spectrum and core level spectra are obtained at a perpendicular take off angle using a pass energy of 150.0 eV (step size 1.00 eV) and 30.0 eV (step size 0.05 eV), respectively. CasaXPS software is used for the deconvolution of core level spectra. A linear background is applied to the Ce spectrum and Shirley background to the Zr, Mn, Ti, O, and Pt spectra. The binding energy is calibrated by placing the principal C 1s peak for adventitious carbon at 284.6 eV. All chemical states of individual elements are assigned according to the binding energy listed in the National Institute of Standards and Technology (NIST) X-ray photoelectron spectroscopy database.[33]

Catalytic Performance Tests. The catalytic activity and durability of the catalyst CZMTO/Pt toward NO reduction are evaluated using a Hiden Analytical CATLAB microreactor system. Thirty milligrams of sample is loaded into a quartz tube end-blocked by quartz wool and loaded into the CATLAB system. A total flow rate of 100 mL/min is applied to the gas mixture for all tests. Gas delivery is controlled by automated mass flow controllers and the reaction temperature measured using a K-type thermocouple inserted into the reactor closely monitored by an automated temperature controller. The outlet gaseous composition is analyzed by a Hiden quadrupole mass spectrometer (QIC20).

The catalyst inside the microreactor prior to the test is purged with helium at a constant flow rate of 88 mL/min, maintaining at 120 °C for 2 h to remove volatile impurities and water. During the catalytic performance test, the reaction gas mixture consisting of 0.06% (600 pm) NO, 0.06% (600 ppm) NH_3, 2.27% O_2, 57.90% N_2, and 39.71% He is delivered to the microreactor and the catalysts are heated from 50 °C at a ramp rate of 6 °C/min. Five cycles of the tests are performed on the Pt-impregnated catalyst heated to 170 °C, while two cycles are performed on the catalyst before Pt impregnation and heating to 220 °C. Between each cycle, the catalyst is allowed to naturally cool down to 50 °C before the next temperature ramping stage is initiated.

The percentage NO conversion at any temperature (T) is calculated using eq 1 on the basis that no reaction occurs at 50 °C

$$\frac{[NO]_{T50} - [NO]_T}{[NO]_{T50}} \times 100 \quad (1)$$

where $[NO]_{T50}$ is the inlet partial pressure of NO at 50 °C of each cycle and $[NO]_T$ is the outlet partial pressure of NO of each cycle at a particular temperature (T) up to 220 and 170 °C for the Pt-impregnated catalyst and pristine catalyst, respectively.

■ ASSOCIATED CONTENT

Supporting Information

The Supporting Information is available free of charge at https://pubs.acs.org/doi/10.1021/acsomega.2c07110.

(Figure S1) XRD patterns of as-synthesized UiO-66 using $ZrCl_4$ and $ZrO(NO_3)_2$ as zirconium precursor; (Figure S2) SEM image and N_2 sorption isotherms at 77 K of as-synthesized UiO-66 using $ZrCl_4$ as zirconium precursor; (Table S1) XPS peak components and attributions for CZMTO/Pt (PDF)

https://doi.org/10.1021/acsomega.2c07110
ACS Omega 2023, 8, 12362−12371

AUTHOR INFORMATION

Corresponding Authors

Kwong-Yu Chan − *Department of Chemistry, The University of Hong Kong, Pokfulam, Hong Kong;* orcid.org/0000-0002-4124-2562; Email: hrsccky@hku.hk

Chi-Ying V. Li − *Department of Chemistry, The University of Hong Kong, Pokfulam, Hong Kong;* orcid.org/0000-0003-2559-9550; Email: cyvli@hku.hk

Authors

Ka-Ming Leung − *Department of Chemistry, The University of Hong Kong, Pokfulam, Hong Kong*

Chi-Kin J. Tsui − *Department of Chemistry, The University of Hong Kong, Pokfulam, Hong Kong*

Ching-Kit Ho − *Department of Chemistry, The University of Hong Kong, Pokfulam, Hong Kong*

Chang-Zhong Liao − *Department of Chemistry, The University of Hong Kong, Pokfulam, Hong Kong; State Key Laboratory of Featured Metal Materials and Life-cycle Safety for composite Structures, School of Resources, Environment and Materials, Guangxi University, Nanning 530004, China*

Hei-Tung Yau − *Department of Chemistry, The University of Hong Kong, Pokfulam, Hong Kong*

Complete contact information is available at: https://pubs.acs.org/10.1021/acsomega.2c07110

Notes

The authors declare no competing financial interest.

ACKNOWLEDGMENTS

The authors thank the Innovation and Technology Commission of the Hong Kong SAR Government for funding through the Innovation and Technology Fund (Project No.: ITS/261/19) and Research Talent Hub (InP/053/20, PiH/231/20, PiH/302/19, PiH/303/19). Publication made possible in part by support from the HKU Libraries Open Access Author Fund sponsored by the HKU Libraries.

REFERENCES

(1) Liu, Y.; Zhao, J.; Lee, J.-M. Conventional and New Materials for Selective Catalytic Reduction (SCR) of NOx. *ChemCatChem.* **2018**, *10*, 1499−1511.

(2) Zhang, S.; Zhang, Q. Surface characterization studies on the interaction of V_2O_5−WO_3/TiO_2 catalyst for low temperature SCR of NO with NH_3. *J. Solid State Chem.* **2015**, *221*, 49−56.

(3) Aguilar-Romero, M.; Camposeco, R.; Castillo, S.; Marin, J.; Rodriguez-Gonzaalez, V.; Garcia-Serrano, L. A.; Mejia-Centeno, I. Acidity, surface species, and catalytic activity study on V_2O_5−WO_3/TiO_2 nanotube catalysts for selective NO reduction by NH_3. *Fuel* **2017**, *198*, 123−133.

(4) Damma, D.; Ettireddy, P. R.; Reddy, B. M.; Smirniotis, P. G. A Review of Low Temperature NH_3-SCR for Removal of NOx. *Catalysts* **2019**, *9*, 349.

(5) Shan, W.; Song, H. Catalysts for the selective catalytic reduction of NOx with NH_3 at low temperature. *Catal. Sci. Technol.* **2015**, *5*, 4280−4288.

(6) Kompio, P. G. W. A.; Bruckner, A.; Hipler, F.; Auer, G.; Loffler, E.; Grunert, W. A new view on the relations between tungsten and vanadium in V_2O_5−WO_3/TiO_2 catalysts for the selective reduction of NO with NH_3. *J. Catal.* **2012**, *286*, 237−247.

(7) Gao, C.; Shi, J.-W.; Fan, Z.; Gao, G.; Niu, C. Sulfur and Water Resistance of Mn-Based Catalysts for Low-Temperature Selective Catalytic Reduction of NOx: A Review. *Catalysts* **2018**, *8*, 11.

(8) Devaiah, D.; Reddy, L. H.; Park, S.-E.; Reddy, B. M. Ceria−zirconia mixed oxides: Synthetic methods and applications. *Catal. Rev.: Sci. Eng.* **2018**, *60*, 177−277.

(9) Shan, Y.; Liu, Y.; Li, Y.; Yang, W. A Review on Application of Cerium-based Oxides in Gaseous Pollutant Purification. *Sep. Purif. Technol.* **2020**, *250*, 117181.

(10) Nolan, M.; Grigoleit, S.; Sayle, D. C.; Parker, S. C.; Watson, G. W. Density functional theory studies of the structure and electronic structure of pure and defective low index surfaces of ceria. *Surf. Sci.* **2005**, *576*, 217−229.

(11) Yang, N.-z.; Guo, R.-t.; Tian, Y.; Pan, W.-g.; Chen, Q.-l.; Wang, Q.-s.; Lu, C.-z.; Wang, S.-x. The enhanced performance of ceria by HF treatment for selective catalytic reduction of NO with NH_3. *Fuel* **2016**, *179*, 305−311.

(12) Gu, T.; Liu, Y.; Weng, X.; Wang, H.; Wu, Z. The enhanced performance of ceria with surface sulfation for selective catalytic reduction of NO by NH_3. *Catal. Commun.* **2010**, *12*, 310−313.

(13) Maitarad, P.; Han, J.; Zhang, D.; Shi, L.; Namuangruk, S.; Rungrotmongko, T. Structure−Activity Relationships of NiO on CeO_2 Nanorods for the Selective Catalytic Reduction of NO with NH3: Experimental and DFT Studies. *J. Phys. Chem. C* **2014**, *118*, 9612−9620.

(14) Qi, G.; Yang, R. T. Performance and kinetics study for low-temperature SCR of NO with NH_3 over MnOx−CeO_2 catalyst. *J. Catal.* **2003**, *217*, 434−441.

(15) Yao, X.; Tang, C.; Gao, F.; Dong, L. Research progress on the catalytic elimination of atmospheric molecular contaminants over supported metal-oxide catalysts. *Catal. Sci. Technol.* **2014**, *4*, 2814−2829.

(16) Zhang, Y.; Tsui, C. J.; Li, C. V.; Chan, K.; Leung, D. Y.; Sit, S. M.; Ho, C.; Leung, K.; Liao, C. Scalable synthesis of ordered mesoporous binary metal oxide: CexZr1-xO2 as thermally stable catalyst for enhanced CO oxidation. *Materials Today Communications* **2021**, *26*, 101811.

(17) Nelson, A. E.; Schulz, K. H. Surface chemistry and microstructural analysis of CexZr1-xO2-y model catalyst surfaces. *Applied Surface Science* **2003**, *210*, 206−221.

(18) Nelson, A. E.; Schulz, K. H. Surface chemistry and microstructural analysis of CexZr1-xO2-y model catalyst surfaces. *Materials Today Communications* **2003**, *210*, 206−221.

(19) Nakajima, F.; Hamada, I. The state-of-the-art technology of NOx control. *Catal. Today* **1996**, *29*, 109−115.

(20) Liu, C.; Chen, L.; Li, J.; Arandiyan, H.; Du, Y.; Xu, J.; Hao, J. Enhancement of Activity and Sulfur Resistance of CeO_2 Supported on TiO_2−SiO_2 for the Selective Catalytic Reduction of NO by NH_3. *Environ. Sci. Technol.* **2012**, *46*, 6182−6189.

(21) Moreno-Tost, R.; Santamarıa-Gonzalez, J.; Rodrıguez-Castellon, E.; Jimenez-Lopez, A. NO reduction with ammonia employing Co/Pt supported on a mesoporous silica containing zirconium as a low temperature selective reduction catalyst. *Applied Catalysis B: Environmental* **2004**, *52*, 241−249.

(22) Bauerie, G.; Wu, S.; Nobe, K. Reduction of Nitric Oxide with Ammonia on Noble Metal Catalysts. *Ind. Eng. Chem. Prod. Res. Dev.* **1975**, *14*, 123−130.

(23) Cai, M.; Bian, X.; Xie, F.; Wu, W.; Cen, P. Preparation and Performance of Cerium-Based Catalysts for Selective Catalytic Reduction of Nitrogen Oxides: A. *Critical Review. Catalysts* **2021**, *11*, 361.

(24) Sutthisripok, W.; Sattayanurak, S.; Sikong, L. Effect of specific surface area on oxygen storage capacity (OSC) and methane steam reforming reactivity of CeO_2. *J. Porous Mater.* **2008**, *15*, 519−525.

(25) Kruk, M.; Jaroniec, M. Gas Adsorption Characterization of Ordered Organic-Inorganic Nanocomposite Materials. *Chem. Mater.* **2001**, *13*, 3169−3183.

(26) Sing, K. S. W.; Williams, R. T. Physisorption Hysteresis Loops and the Characterization of Nanoporous Materials. *Adsorption Science & Technology* **2004**, *22*, 773−783.

(27) Katz, M. J.; Brown, Z. J.; Colon, Y. J.; Siu, P. W.; Scheidt, K. A.; Snurr, R. Q.; Hupp, J. T.; Farha, O. K. A facile synthesis of UiO-66, UiO-67 and their derivatives. *Chem. Commun.* **2013**, *49*, 9449−9451.
(28) Zhang, L.; Wu, H. B.; Lou, X. W. D. Metal-Organic-Frameworks-Derived General Formation of Hollow Structures with High Complexity. *J. Am. Chem. Soc.* **2013**, *135*, 10664−10672.
(29) Paunovic, N.; Dohcevic-Mitrovic, Z.; Scurtu, R.; Askrabic, S.; Prekajski, M.; Matovic, B.; Popovic, Z. V. Suppression of inherent ferromagnetism in Pr-doped CeO_2 nanocrystals. *Nanoscale* **2012**, *4*, 5469−5476.
(30) Zou, H.; Yao, Q.; Huang, M.; Zhu, M.; Zhang, F.; Lu, Z.-H. Noble-metal-free NiFe nanoparticles immobilized on nano $CeZrO_2$ solid solutions for highly efficient hydrogen production from hydrous hydrazine. *Sustainable Energy Fuels* **2019**, *3*, 3071−3077.
(31) Zhang, B.; Zhang, S.; Liu, B. Effect of oxygen vacancies on ceria catalyst for selective catalytic reduction of NO with NH_3. *Appl. Surf. Sci.* **2020**, *529*, 147068.
(32) Zhang, B.; Liebau, M.; Liu, B.; Li, L.; Zhang, S.; Glaser, R. Selective catalytic reduction of NOx with NH_3 over Mn-Zr-Ti mixed oxide catalysts. *J. Mater. Sci.* **2019**, *54*, 6943−6960.
(33) Naumkin, A. V.; Kraut-Vass, A.; Gaarenstroom, S. W.; Powell, C. J. *NIST X-ray Photoelectron Spectroscopy Database, NIST Standard Reference Database Number 20*; National Institute of Standards and Technology: Gaithersburg, MD, 2000.

https://doi.org/10.1021/acsomega.2c07110
ACS Omega 2023, 8, 12362−12371